The effect of gold nanoparticle capping agents on 1O2 detection by singlet oxygen sensor green

Sarra Mitiche, Jean-Frédéric Audibert, Sylvie Marguet, Bruno Palpant, Robert Bernard Pansu

The Effect of Gold Nanoparticle Capping Agents on $^1O_2$ Detection by Singlet Oxygen Sensor Green

Sarra Mitiche [a*], Jean-FrédéricAudibert [b], Sylvie Marguet [c], Bruno Palpant [a], Robert Bernard Pansu [a]

[a] Université Paris-Saclay, CNRS, ENS Paris-Saclay, CentraleSupélec, LuMIn, 91190Gif-sur-Yvette, France.
[b] Université Paris-Saclay, CNRS, ENS Paris-Saclay, PPSM, 91190Gif-sur-Yvette, France.
[c] Université Paris-Saclay, CEA, CNRS, NIMBE, 91190Gif-sur-Yvette, France.

*Corresponding author.
E-mail address:sarra.mitiche-berkouk@centralesupelec.fr

Abstract:

Singlet Oxygen Sensor Green (SOSG) is the most widely used fluorescent probe for detecting singlet oxygen ($^1O_2$). $^1O_2$ can be efficiently produced by exciting the surface plasmon of gold nanoparticles with laser pulses. However, gold nanoparticles are usually embedded in a chemical stabilizer that can interact with SOSG, leading to erroneous detection of $^1O_2$. This article shows that the emission properties of SOSG strongly depend on the concentration of cetyltrimethylammonium bromide (CTAB), a capping agent widely used for nanoparticles synthesis and stabilization. The sensitivity of SOSG to $^1O_2$ is also drastically affected by the presence of CTAB. This effect is due to the fluorescent probe's aggregation in CTAB premicellar aggregates and micelles, and the change in the probe configuration. Furthermore, the behavior of SOSG in the presence of two other widely-used surfactants, i.e., citrate and Polyethylene Glycol (PEG), is investigated to determine the right nanoparticle stabilizer to use with SOSG probe.

Keywords:

Singlet Oxygen Sensor Green (SOSG), Singlet oxygen, Reactive Oxygen Species (ROS), Surface plasmon resonance, CTAB, Fluorescent sensor.

1. Introduction:

At nanometer scale, gold exhibits a remarkable optical phenomenon: the localized surface plasmon resonance (LSPR). This denotes the collective oscillation of the conduction electrons in a metallic nanoparticle (MNP) under light excitation [1, 2]. The resonance characteristics of this oscillation depend on the nanoparticle parameters like the shape or the size and the refractive index of the surrounding medium.Currently, LSPR offers great promises for photodynamiccancer therapy [3, 4]. Indeed, it has been demonstrated that upon irradiation at LSPR wavelength, MNPs can produce, in a biological medium, reactive oxygen species (ROS) [5, 6]that can induce necrosis and apoptosis of cells [7, 8, 9, 10, 11]. Thanks to their reduced cytotoxicity, high accumulation in tumors and good resistance to photobleaching and enzymatic degradation [12, 13], MNPs would be good substitutes for the chemical photosensitizers commonly employed in Photo-Dynamic Therapy (PDT). Moreover, MNPs are more effective than chemical photosensitizers [14] due to the possibility to adjust the MNPs parameters to have a high absorption in the therapeutic spectral window (650 to 1350 nm [15]).

Singlet oxygen ($^1O_2$) [16, 17] is the most effective ROS in destroying cancer cells and is widely used in PDT [18, 19]. Singlet oxygen can be detected using fluorescent probes [20, 21], the most selective one being the Singlet Oxygen Sensor Green (SOSG) [22]. SOSG sensor exhibits weak blue fluorescence, with excitation maxima at 372 and 393 nm and emission peaks at 395 and 416 nm. After reaction with singlet oxygen, it emits a green fluorescence with an excitation/emission maximum at 504/525 nm [23]. According to previous reports [24, 25, 26], SOSG is composed of an anthracene

chromophore and a fluorescein one. In the absence of singlet oxygen, SOSG green emission is quenched by an internal electron transfer from the anthracene moiety to fluorescein. In the presence of $^1O_2$, an endoperoxideis formed by the interaction between $^1O_2$ and the anthracene moiety, the internal electron transfer does not occur, and the fluorescein is fluorescent. SOSG is widely used in many fields, including biochemistry, botany and medical science [22, 27, 28] due to its high selectivity for $^1O_2$. However, care must be taken when using it since the characteristics and the composition of the solvent employed can alter the florescence of the molecule. Indeed, emission of SOSG can be turned on at alkaline pH or in the presence of some solvents like acetonitrile, dimethyl sulfoxide (DMSO), dimethylformamide (DMF) and acetone [23]. Moreover, it has been demonstrated that SOSG is not a suitable probe for $^1O_2$ in the presence of ionizing radiation [29], and it can also produce $^1O_2$ by itself under a photoirradiation [24]. Usually, investigations of singlet oxygen generation assisted by surface plasmons are conducted using MNPs in aqueous solution and embedded in a chemical capping agent (cetyltrimethylammonium bromide (CTAB) [30], citrate [31, 32], Polyethylene Glycol (PEG) [33], etc.) to ensure nanoparticle colloidal stability. Regarding the above-listed SOSG limitations, the fluorescence of the probe could be altered by the used surfactant and thuscould lead to a misinterpretation of the results.

In the present article, we investigate the behavior of the SOSG sensor in the presence of CTAB, a capping agent widely used for MNPs stabilization. The fluorescence of SOSG dissolved in CTAB aqueous solutions of various concentrations is recorded using an epifluorescence microscope.We demonstrate that the emission properties of the SOSG sensor depend highly on the CTAB concentration. Indeed, we show through SOSG emission spectra and SOSG time-resolved fluorescence decays that SOSG molecules are trapped in CTAB micelles and pre-micellar aggregates; the emission properties of the probe are thus modulated by the CTAB aggregation state. Fluorescence measurements are also conducted in the presence of gold nanorods (AuNRs) acting as $^1O_2$ photosensitizers, and embedded in various capping agents: CTAB, citrate and PEG.We show that singlet oxygen detection is not possible in the presence of CTAB whereas a high sensitivity of SOSG for $^1O_2$ is noted in citrate and PEG. We conclude that citrate and PEG are the most effective capping agents to use with the SOSG for the investigation of singlet oxygen generation by surface plasmons.

2. Materials and methods

2.1. AuNRs synthesis

Single-crystalline gold nanorods (AuNRs), stabilized by the CTAB surfactant, are synthesized by colloidal chemistry using the so-called *seed-mediated growth method* (see the reference [34] for a recent comprehensive review of this technique). We used the improved seed-mediated method reported by the Murray's group [35] to synthesize very monodisperse AuNRs of 13±0.5 nm thick and 77±5 nm long, corresponding to a plasmon resonance peak at 1033 nm in water (1 mM CTAB). CTAB molecules form a tightly bound bilayer on the gold surfacebecause bromide ions, as all halide ions, have a strong affinity to chemisorb on the gold surface [36]. Therefore, the replacement of CTAB molecules by other surfactants, such as the weakly bound citrate molecule, is not an easy task because aggregation at the nanoscale takes place spontaneously in the absence of special precautions. In the present work, CTAB replacement by citrate and polyethylene glycol (PEG) is performed using the efficient ligand exchange procedure developed by the Wei's group, based on polystyrenesulfonate (PSS) as an intermediate surfactant [37]. PEG is a biocompatible polymer often used in cancer therapy to improve the biodistribution of the nanoparticles [38] because PEGylated AuNRs are stable in biological fluids (high ionic strength) and present stealth properties [39]. PEG is known to lengthen the circulation time in the blood stream by reducing the adsorption of proteins, thus preventing their clearance by the mononuclear phagocytic system, also known as reticuloendothelial system [40]. Detailed protocols for the AuNRs synthesis and surface modification can be found in the electronic supplementary material.

2.2. Sample preparation

A stock solution of 10 mM CTAB is prepared by dissolving solid CTAB ($[(C_{16}H_{33})N(CH_3)_3]Br$) in deionized water *Milli-Q*. The obtained solution is heated in a water bath at temperature below 100°C in order to dissolve CTAB crystals. CTAB solutions of 0.1, 0.3, 1, 3 and 5 mM are obtained by diluting the 10 mM one. The solutions are heated again in a water bath to well dissolve the CTAB. For the experimental purpose, 988 µl are taken from each solution and 10 µl of Tris-HCl buffer at pH=6.5 are added to them in order to ensure pH stability. SOSG is provided in vials containing 100 µg of product. The 100 µg of solid SOSG are dissolved in 33 µl of methanol to obtain a stock solution of about 5 mM [23]. 2 µl of SOSG solution are added to the CTAB/Tris-HCl mixtures to have 1 ml of solution with a concentration of SOSG equal to 10 µM.

The stock solution containing AuNRs in 5mM CTAB is heated in a water bath to avoid CTAB crystals. 998 µl are taken from it and 2 µl of dissolved SOSG are added to have a final solution of 1 ml with 10 µM of SOSG. The stock solution of Au-rod in 5mM citrate contains 0.5% of NaOH 0.1M to prevent from nanoparticles aggregation. The pH of the solution is 9. To avoid the activation of SOSG by the alkaline pH, 10µl of $NaH_2PO_4.2H_2O$ 0.1M are added to 988 µl of the stock solution just before the addition of 2 µl of SOSG and the experiment. Finally, we obtain 1 ml of solution at pH=7.5 containing AuNRs in 5 mM citrate and SOSG with a concentration of 10 µM. Finally, the 1 ml of AuNRs in PEG with 10 µM of SOSG are prepared by mixing 998 µl of the AuNRs in PEG stock solution and 2 µl of the dissolved SOSG.

Samples are prepared by sucking the solution into a square borosilicate capillary (*VitroTubes*, Product n° 8100, length 100mm, square ID 1 mm, wall 0.2 mm, square OD 1.4 mm [41]).The capillary is then sealed with two putty plugs (Fig.1).The method of inserting the drop into the capillary is summarized in the electronic supplementary material.

2.3. Experiment

The fluorescence of the sample is recorded using an epifluorescence microscope (*TE2000-U, Nikon*). The sample is positioned at the objective focal plane (*CFI Plan Apo DM Lambda 60XC, N.A. 0.94*) and illuminated through it in widefield mode. The emitted light is collected through the same objective. A fraction of the collected light is sent to a CCD camera (*Retiga R1, QImaging* [42]) for a real-time visualization of the sample fluorescence. The other part is collected by a spectrometer (*Maya 2000 Pro, OceanOptics*[43]) to register the emission spectrum. For fluorescence lifetime imaging, light is sent to a time and space-resolved single photon counter (TCSPC detector, prototype obtained from the Leibniz Institute for Neurobiology of Magdeburg [44]). In this setup, AuNRs are excited at 1030 nm (1.2 eV), corresponding to their longitudinal LSPR, with the pulsed output of a femtosecond Yb:KGW laser (*t-pulse 200, Amplitude Systèmes*, repetition rate 10 MHz, pulse width 400 fs). The polarization of the beam is circular to excite the randomly oriented nanoparticles. The peak power density at the sample surface is tuned from 160 to 1700 MW/cm^2. The SOSG probe is excited with a laser beam at 515 nm wavelength (2.4 eV), SHG is generated by focalizing the 1030 nm beam into a nonlinear crystal of β-BaB_2O_4. The diameters of illumination profiles at the sample plane are 25 µm@$1/e^2$ and 45 µm@$1/e^2$ for 1030 nm and 515 nm, respectively. The experimental setup is summarized in Fig. 1.

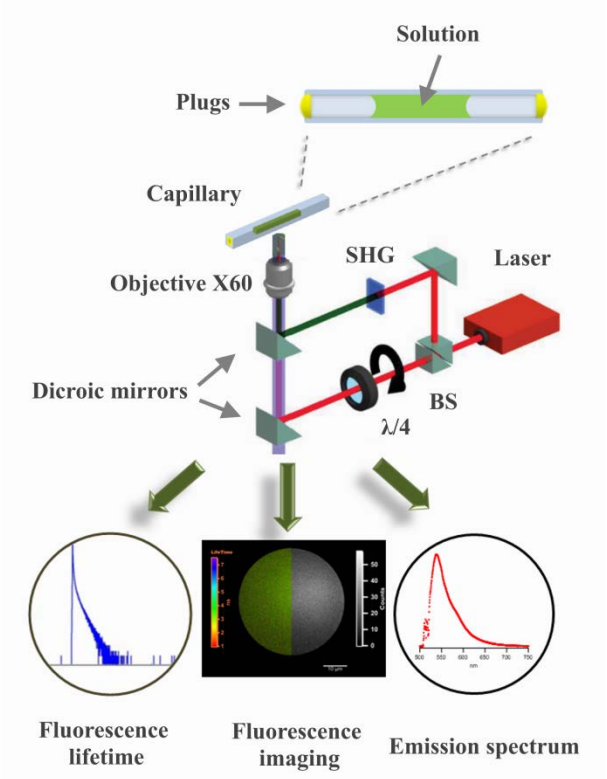

Fig. 1. Schematic representation of the sample and the experimental setup. SHG: Second Harmonic Generation, BS: Beam Splitter.

3. Results and discussion:

3.1. SOSG in CTAB aqueous solutions

The emission intensity and emission spectra (see the electronic supplementary material) of SOSG in CTAB aqueous solutions of 0, 0.1, 0.3, 1, 3 and 10 mM are recorded for an excitation wavelength of 515 nm. The evolutions of the emission intensity and emission wavelength with CTAB concentration are depicted in Figs. 2a and 2b, respectively. A noticeable SOSG emission is registered in the absence of an external $^1O_2$ photosensitizer. This initial emission is presumably due to the presence of some impurities and the formation of endoperoxides as a result of the synthesis of singlet oxygen by SOSG upon an irradiation at 515 nm [24]. SOSG emission intensity decreases as CTAB concentration slightly increases from 0 mM (water) to 0.3 mM. This decrease in emission intensity is accompanied by a red shift of the emission wavelength. An increase of the emission intensity is noted for CTAB concentrations beyond the CTAB critical micellar concentration (CMC) in distilled water (CMC~0.9 mM at 25°C [45]); the emission wavelength is shifted to the blue. For higher CTAB concentrations, the emission intensity and the emission wavelength reach a plateau. Additional data are provided in the electronic supplementary material to validate reproducibility of the results. The data reported in Figs. 2a and 2b show that the emission properties of SOSG depend highly on CTAB concentration. The modifications observed in the SOSG emission wavelength pinpoint changes in the surrounding environment of the molecules. As most surfactants, CTAB in aqueous solutions forms pre-micellar aggregates and then micelles around impurities as its concentration raises. As a result, the variations observed in SOSG emission wavelength and intensity while CTAB concentration increases are most probably due to the enclosing of the SOSG molecules in CTAB pre-micellar aggregates and micelles.

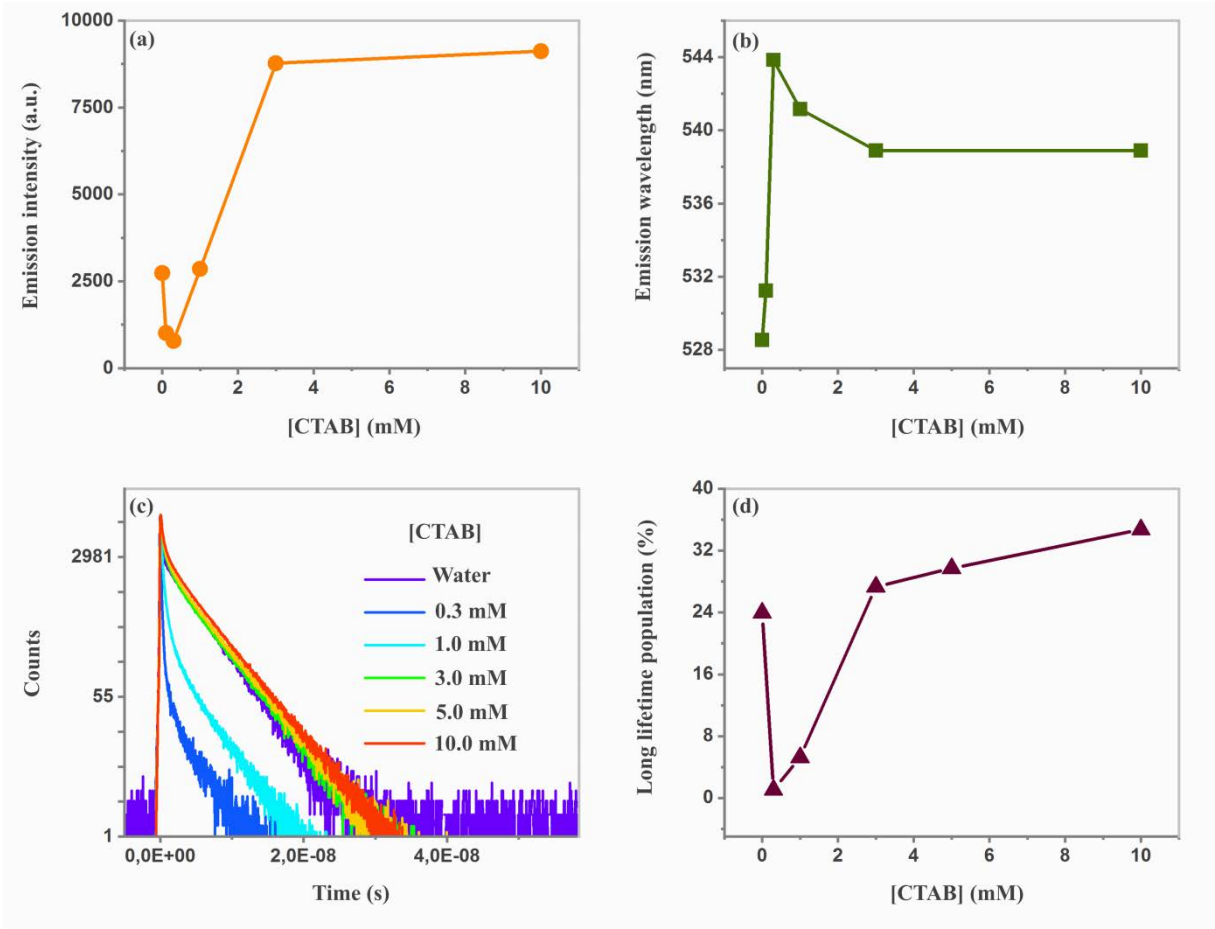

Fig. 2. SOSG in various concentrated CTAB aqueous solutions. (a) SOSG emission intensity and (b) SOSG emission wavelength. as a function of CTAB concentration. (c) SOSG time-resolved fluorescence decays. (d) Relative population of theSOSG molecules with long emission lifetime as a function of CTAB concentration. The excitation wavelength is 515nm.

To further understand the effect of CTAB aggregation on SOSG emission properties, time-resolved fluorescence decays of SOSG in CTAB aqueous solutions of 0, 0.3, 1, 3, 5 and 10 mM are recorded for an excitation wavelength of 515 nm. The results are presented in Fig. 2c. The decays show the presence of SOSG molecules with a long emission lifetime and others with a short emission lifetime. Molecules with a short emission lifetime are those whose emission is quenched either by the internal electron transfer between the anthracene and fluorescein moiety or by the presence of neighboring SOSG molecules. The population with a long emission lifetime (3.5 ns) is that of the unquenched fluorescein moiety. It can be impurities or oxidized SOSG molecules or extended conformations [46] of SOSG in the CTAB micelle. It is responsible for the emission displayed in Fig. 2a. The relative population of molecules with a long emission lifetime according to CTAB concentration is depicted in Fig. 2d. For CTAB concentrations below the CTAB CMC (< 1mM), the quantity of molecules with a long emission lifetime decreases when CTAB concentration slightly increases. This phenomenon is due to the formation of positively-charged pre-micellar CTAB aggregates which trap the anionic SOSG molecules by electric attraction. SOSG molecules accumulate into CTAB aggregates, and the emission of each molecule is quenched by the adjacent ones. From the CMC, SOSG molecules are enclosed in CTAB micelles and the relative number of molecules with a long emission lifetime increases because the number of SOSG molecules per micelle decreases. Indeed, at a concentration of 2 mM CTAB, the concentration of micelles is 11 µM and exceeds the concentration of SOSG molecules of 10 µM, so, the probability to have a single SOSG molecule in a CTAB micelle rises. As a result, the probability of emission self-quenching between close-lying SOSG molecules decreases, which explains the rise of SOSG emission intensity (Fig. 2a). To summarize, the variation of the CTAB aggregation state modulates the emission properties of the SOSG. This phenomenon has also been reported for other fluorescent molecules [47, 48] and has been used to measure micelles aggregation numbers [49].

3.2. SOSG with AuNRs

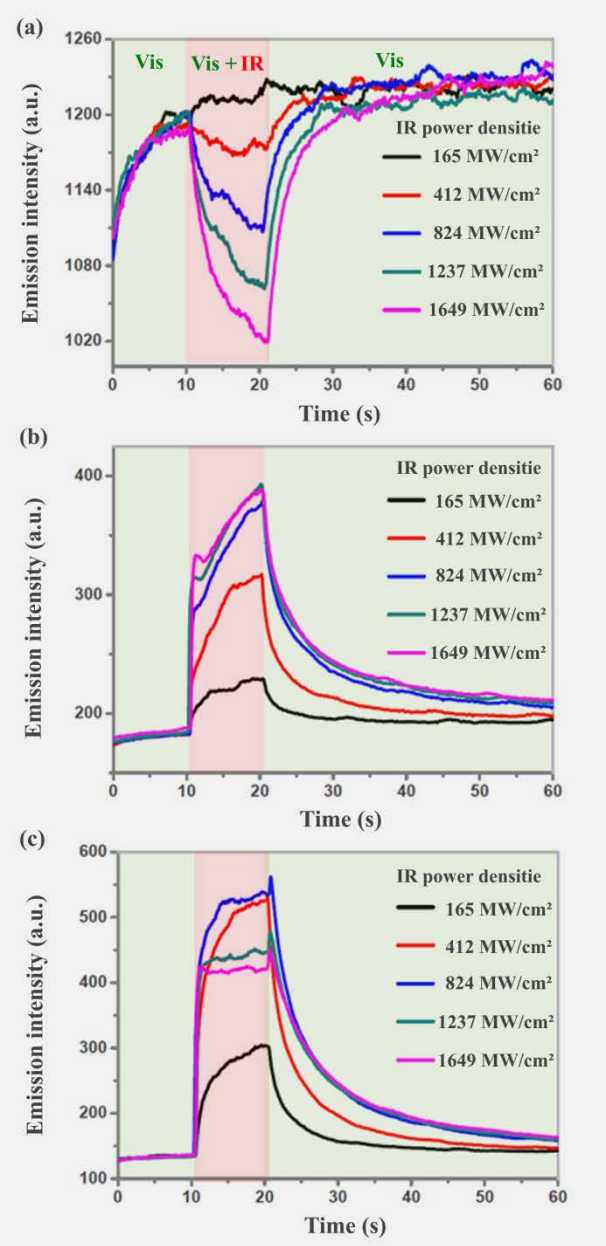

Fig.3. SOSG emission intensity in the presence of AuNRs acting as $^1O_2$ photosensitizers and embedded in various capping agents (a) 5 mM CTAB, (b) 5 mM citrate, (c) PEG. The SOSG fluorescence is recorded before, during and after the excitation of the longitudinal LSPR of the AuNRs (λ_{LSPR} = 1030 nm) with IR power densities ranging from 165 to 1650 MW/cm². The SOSG probe is excited at 515 nm wavelength.

We have previously demonstrated that the aggregation state of CTAB modifies the emission properties of SOSG. In this section, we determine the effect of CTAB concentration on the sensitivity of SOSG to singlet oxygen. For this purpose, SOSG emission intensity is recorded in the presence of AuNRs acting as $^1O_2$ photosensitizers. The results are compared to those obtained by replacing CTAB by two other capping agents: citrate and PEG. The used AuNRs have 77±5 nm in length and 13±1 nm in diameter; a SEM image is given in the electronic supporting material. The AuNRs are dispersed in an aqueous solution composed of 10 µM of SOSG and 5 mM of CTAB. According to the SOSG emission intensity curve (Fig. 2a), a CTAB concentration of 5 mM allows the dispersion of SOSG

molecules in CTAB micelles and thus prevents from the emission self-quenching between them. For CTAB concentrations beyond 5mM, foam is formed which complicates the experiment. The longitudinal LSPR of the AuNRs in CTAB peaks at 1033 nm, and the corresponding extinction spectrum is provided in the electronic supplementary material. The sample is first illuminated at 515 nm wavelength for 10s so as to record the initial emission intensity of SOSG. A laser beam at 1030 nm wavelength is then added to the 515 nm one for 10s to excite the longitudinal LSPR of the AuNRs and generate $^1O_2$ by surface plasmon [13, 27]. Finally, the 1030 nm laser beam is turned off and the emission of SOSG after the excitation of surface plasmon is registered. The SOSG emission intensity is recorded for IR power densities ranging from 165 to 1650 MW/cm². The power density of the laser beam at 515 nm is about 0.5 MW/cm².The experiment is repeated with AuNRs in 5 mM citrate and PEG with a longitudinal LSPR at 1014 nm and 1030 nm, respectively (extinction spectra are reported in the electronic supporting material). The results are displayed in Fig. 3.

An initial SOSG emission under the irradiation at 515 nm is observed in the three solutions before the excitation of surface plasmons. The intensity of this initial SOSG fluorescence rises exponentially at a rate depending on the used capping agent ($\tau_{CTAB} > \tau_{PEG}, \tau_{Citrate}$). The initial fluorescence in CTAB is about 7 times higher than in citrate or PEG. The rise of the SOSG fluorescence intensity when the solution is irradiated at 515 nm is due to the reaction of the triplet state of SOSG with oxygen. The oxidation can be either direct or induced by the formation of $^1O_2$ that further reacts with SOSG. The higher fluorescence yield in CTAB compared to citrate and PEG can be explained by the separation of the two parts of the SOSG molecule (fluorescein and anthracene) by the micelle [50], which favors the presence of an open conformer of the probe without intramolecular electron transfer and the 3.5 ns lifetime of the unquenched fluorescein. During the excitation of the longitudinal LSPR of the AuNRs, an increase of the SOSG emission is observed for citrate and PEG (Figs. 3b and 3c, respectively) indicating the generation of singlet oxygen by surface plasmons. In the CTAB solution (Fig. 3a), no augmentation of the SOSG emission intensity is registered while producing $^1O_2$. On the contrary, a decrease in the SOSG fluorescence is observed when the power density of the 1030 nm laser beam increases. The singlet oxygen produced by the AuNRs can react with SOSG, either by the formation of an endoperoxide and the SOSG molecule becomes fluorescent, or by the oxidation of the fluorescein moiety which gives a non-fluorescent SOSG molecule:

$$\begin{Bmatrix} F-A \\ \subset FA \end{Bmatrix} + {}^1O_2 \rightarrow \begin{Bmatrix} FO-A+F-AO \\ \subset FOA + \subset FAO \end{Bmatrix}$$

where $F-A$and $\subset FA$ (F: fluorescein, A: anthracene) are the open and close conformer of SOSG, respectively, $F-AO$ and $\subset FAO$ the SOSG oxidized on the anthracene moiety (fluorescent molecules),$\subset FOA$ and $FO-A$ the SOSG oxidized on the fluorescein moiety (non-fluorescent molecules). In the case of citrate and PEG, the number of fluorescent SOSG molecules before the excitation of surface plasmons is negligible, so, the SOSG molecules oxidized through the capture of singlet oxygen by the fluorescein moiety $\subset FOA$ (non-fluorescent molecules) are not detected and only the rise of SOSG emission due to the oxidation of the anthracene moiety ($\subset FAO$) is observed. However, in the CTAB solution, because of the modification of the conformation of the SOSG molecules by the CTAB micelles ($\subset FA \rightarrow F-A$), the number of fluorescent molecules before the generation of $^1O_2$ by the AuNRs is large, and the decrease of the SOSG emission during the excitation of surface plasmons is due to the capture of singlet oxygen by the fluorescein moiety ($FO-A$). For lower CTAB concentrations, the SOSG fluorescence before and during the synthesis of $^1O_2$ remains constant because of the emission self-quenching between neighboring SOSG molecules. As an example, the results of the experiment conducted at a CTAB concentration of 1 mM are given in the electronic supplementary material. After switching off the laser at 1030 nm, the SOSG emission

intensity returns gradually to its initial value as a result of the diffusion of the oxidized SOSG molecules outside the field of view. Additional data are given in the electronic supplementary material to validate the results reproducibility. The results of Fig. 3 show that the ability of the SOSG probe to detect $^1O_2$ is strongly affected by the CTAB concentration so we conclude that citrate and PEG are much more effective than CTAB as capping agents to use with SOSG.

4. Conclusion

In summary, we have demonstrated that the emission properties of SOSG and its sensitivity to singlet oxygen are strongly affected by the presence of CTAB. At low CTAB concentrations, the SOSG fluorescence is killed by the formation of CTAB premicellar aggregates that trap the probe and singlet oxygen cannot be detected. For larger concentrations, the fluorescence of the unreacted probe in the CTAB micelles is increased; as a result, the release of singlet oxygen is associated with a drop of the fluorescence. CTAB is one of the mostly used stabilizer for gold nanoparticles and the use of SOSG with it in the investigation of singlet oxygen generation assisted by surface plasmon can lead to erroneous results. Another alternative to CTAB is the use of citrate or Polyethylene Glycol (PEG) as capping agent.

Acknowledgements

The authors acknowledge the financial support received from the “Plan Cancer” managed by the French ITMO Cancer (n°17CP077–00, project HEPPROS). This work is also supported by a public grant overseen by the French National Research Agency (ANR) as part of the “Investissements d’Avenir” program (reference: ANR-10- LABX-0035, Labex NanoSaclay). The support of Jacques Peixoto in time-resolved fluorescence decay measurements was greatly appreciated.

Appendix. Supplementary data

Electronic supplementary material related to this article is available at https://doi.org/10.1016/.....

References:

[1] M.A. Garcia, Surface plasmons in metallic nanoparticles: fundamentals and applications Surface Plasmons in metallic nanoparticles, Phys. D Appl. Phys. 44 (2011) 283001. https://doi.org/10.1088/0022.

[2] S.A. Maier, Plasmonics: Fundamentals and Applications, Springer US, New York, 2007.

[3] S. Kwiatkowski, B. Knap, D. Przystupski, J. Saczko, E. Kędzierska, K. Knap-Czop, J. Kotlińska, O. Michel, K. Kotowski, J. Kulbacka, Photodynamic therapy – mechanisms, photosensitizers and combinations, Biomed. Pharmacother. 106 (2018) 1098–1107. https://doi.org/10.1016/j.biopha.2018.07.049.

[4] D.E.J.G.J. Dolmans, D. Fukumura, R.K. Jain, Photodynamic therapy for cancer, Nat. Rev. Cancer. 3 (2003) 380–387. https://doi.org/10.1038/nrc1071.

[5] M. Suzuki, S. Yamamoto, Handbook on reactive oxygen species (ROS) : formation mechanisms, physiological roles and common harmful effects, Nova Science Publishers, 2014.

[6] C. Filip, E. Albu, Reactive oxygen species (ROS) in living cells, InTech, 2018.

[7] T. Labouret, Irradiation laser ultrabrève de nanobâtonnets d'or individuels en milieu aqueux : photo-génération de phénomènes d'intérêt biomédical, Doctoral dissertation, Paris-Saclay University, 2016.

[8] T. Labouret, J.F. Audibert, R.B. Pansu, B. Palpant, Plasmon-Assisted Production of Reactive Oxygen Species by Single Gold Nanorods, Small. 11 (2015) 4475–4479. https://doi.org/10.1002/smll.201500509.

[9] L. Gao, R. Liu, F. Gao, Y. Wang, X. Jiang, X. Gao, Plasmon-mediated generation of reactive oxygen species from near-infrared light excited gold nanocages for photodynamic therapy in vitro, ACS Nano. 8 (2014) 7260–7271. https://doi.org/10.1021/nn502325j.

[10] S.J. Chadwick, D. Salah, P.M. Livesey, M. Brust, M. Volk, Singlet oxygen generation by laser irradiation of gold nanoparticles, J. Phys. Chem. C. 120 (2016) 10647–10657. https://doi.org/10.1021/acs.jpcc.6b02005.

[11] Y. Feng, Y. Chang, X. Sun, Y. Cheng, R. Zheng, X. Wu, L. Wang, X. Ma, X. Li, H. Zhang, Differential photothermal and photodynamic performance behaviors of gold nanorods, nanoshells and nanocages under identical energy conditions, Biomater. Sci. 7 (2019) 1448–1462. https://doi.org/10.1039/c8bm01122b.

[12] J.P. Liu, T.T. Wang, D.G. Wang, A.J. Dong, Y.P. Li, H.J. Yu, Smart nanoparticles improve therapy for drug-resistant tumors by overcoming pathophysiological barriers, Acta Pharmacol. Sin. 38 (2017) 1–8. https://doi.org/10.1038/aps.2016.84.

[13] R. Vankayala, A. Sagadevan, P. Vijayaraghavan, C.-L. Kuo, K.C. Hwang, Metal Nanoparticles sensitize the formation of singlet oxygen, Angew. Chemie Int. Ed. 50 (2011) 10640–10644. https://doi.org/10.1002/anie.201105236.

[14] R. Vankayala, Y.-K. Huang, P. Kalluru, C.-S. Chiang, K.C. Hwang, First demonstration of gold nanorods-mediated photodynamic therapeutic destruction of tumors via near infra-red light activation, Small. 10 (2014) 1612–1622. https://doi.org/10.1002/smll.201302719.

[15]A.M. Smith, M.C. Mancini, S. Nie, Bioimaging: Second window for in vivo imaging, Nat. Nanotechnol. 4 (2009) 710–711. https://doi.org/10.1038/nnano.2009.326.

[16]P.R. Ogilby, Singlet oxygen: There is indeed something new under the sun, Chem. Soc. Rev. 39 (2010) 3181–3209. https://doi.org/10.1039/b926014p.

[17] M.C. DeRosa, R.J. Crutchley, Photosensitized singlet oxygen and its applications, Coord. Chem. Rev. 233–234 (2002) 351–371. https://doi.org/10.1016/S0010-8545(02)00034-6.

[18] L. Pinto da Silva, A. Núnez-Montenegro, C.M. Magalhães, P.J.O. Ferreira, D. Duarte, P. González-Berdullas, J.E. Rodríguez-Borges, N. Vale, J.C.G. Esteves da Silva, Single-molecule chemiluminescent photosensitizer for a self-activating and tumor-selective photodynamic therapy of cancer, Eur. J. Med. Chem. 183 (2019) 111683. https://doi.org/10.1016/j.ejmech.2019.111683.

[19] H. Guo, H. Qian, N.M. Idris, Y. Zhang, Singlet oxygen-induced apoptosis of cancer cells using upconversion fluorescent nanoparticles as a carrier of photosensitizer, Nanomedicine Nanotechnology, Biol. Med. 6 (2010) 486–495. https://doi.org/10.1016/j.nano.2009.11.004.

[20] N. Soh, Recent advances in fluorescent probes for the detection of reactive oxygen species, Anal. Bioanal. Chem. 386 (2006) 532–543. https://doi.org/10.1007/s00216-006-0366-9.

[21] É. Hideg, A comparative study of fluorescent singlet oxygen probes in plant leaves, Cent. Eur. J. Biol. 3 (2008) 273–284. https://doi.org/10.2478/s11535-008-0018-5.

[22] C. Flors, M. J. Fryer, J. Waring, B. Reeder, U. Bechtold, P. M. Mullineaux, S. Nonell, M. T. Wilson, N. R. Baker, Imaging the production of singlet oxygen *in vivo* using a new fluorescent sensor, Singlet Oxygen Sensor Green, J. Exp. Bot.57 (2006)1725–1734.https://doi.org/10.1093/jxb/erj181.

[23] Molecular Probes Product Information, 2004.

[24] X. Ragàs, A. Jiménez-Banzo, D. Sánchez-García, X. Batllori, S. Nonell, Singlet oxygen photosensitisation by the fluorescent probe Singlet Oxygen Sensor Green®, Chem. Commun. 20(2009) 2920–2922. https://doi.org/10.1039/b822776d.

[25] S. Kim, M. Fujitsuka, T. Majima, Photochemistry of singlet oxygen sensor green, J. Phys. Chem. B. 117 (2013) 13985–13992. https://doi.org/10.1021/jp406638g.

[26] A. Gollmer, J. Arnbjerg, F.H. Blaikie, B.W. Pedersen, T. Breitenbach, K. Daasbjerg, M. Glasius, P.R. Ogilby, Singlet oxygen sensor green®: Photochemical behavior in solution and in a mammalian cell, Photochem. Photobiol. 87 (2011) 671–679. https://doi.org/10.1111/j.1751-1097.2011.00900.x.

[27] Y. Zhang, K. Aslan, M.J.R. Previte, C.D. Geddes, Plasmonic engineering of singlet oxygen generation, Proc. Natl. Acad. Sci. U. S. A. 105 (2008) 1798–1802. https://doi.org/10.1073/pnas.0709501105.

[28] Y. Osakada, K. Kawai, T. Tachikawa, M. Fujitsuka, K. Tainaka, S. Tero-Kubota, T. Majima, Generation of singlet oxygen during photosensitized one-electron oxidation of DNA, Chem. - A Eur. J. 18 (2012) 1060–1063. https://doi.org/10.1002/chem.201101964.

[29] H. Liu, P.J.H. Carter, A.C. Laan, R. Eelkema, A.G. Denkova, Singlet Oxygen Sensor Green is not a suitable probe for $^1O_2$ in the presence of ionizing radiation, Sci. Rep. 9 (2019) 1–8. https://doi.org/10.1038/s41598-019-44880-2.

[30] J. Rodríguez-Fernández, J. Pérez-Juste, P. Mulvaney, L.M. Liz-Marzán, Spatially-directed oxidation of gold nanoparticles by Au(III)-CTAB complexes, J. Phys. Chem. B. 109 (2005) 14257–14261. https://doi.org/10.1021/jp052516g.

[31] N. Hanžić, T. Jurkin, A. Maksimović, M. Gotić, The synthesis of gold nanoparticles by a citrate-radiolytical method, Radiat. Phys. Chem. 106 (2015) 77–82. https://doi.org/10.1016/j.radphyschem.2014.07.006.

[32] H. Du Toit, T.J. Macdonald, H. Huang, I.P. Parkin, A. Gavriilidis, Continuous flow synthesis of citrate capped gold nanoparticles using UV induced nucleation, RSC Adv. 7 (2017) 9632–9638. https://doi.org/10.1039/c6ra27173a.

[33] J. Manson, D. Kumar, B.J. Meenan, D. Dixon, Polyethylene glycol functionalized gold nanoparticles: The influence of capping density on stability in various media, Gold Bull. 44 (2011) 99–105. https://doi.org/10.1007/s13404-011-0015-8.

[34] Y. Xia, K.D. Gilroy, H.C. Peng, X. Xia, Seed-mediated growth of colloidal metal nanocrystals, Angew. Chemie - Int. Ed. 56 (2017) 60–95. https://doi.org/10.1002/anie.201604731.

[35] X. Ye, C. Zheng, J. Chen, Y. Gao, C.B. Murray, Using binary surfactant mixtures to simultaneously improve the dimensional tunability and monodispersity in the seeded growth of gold nanorods, Nano Lett. 13 (2013) 765–771. https://doi.org/10.1021/nl304478h.

[36] B. Nikoobakht, M.A. El-Sayed, Evidence for bilayer assembly of cationic surfactants on the surface of gold nanorods, Langmuir. 17 (2001) 6368–6374. https://doi.org/10.1021/la010530o.

[37] J.G. Mehtala, D.Y. Zemlyanov, J.P. Max, N. Kadasala, S. Zhao, A. Wei, Citrate-stabilized gold nanorods, Langmuir. 30 (2014) 13727–13730. https://doi.org/10.1021/la5029542.

[38] N.S. Abadeer, C.J. Murphy, Recent progress in cancer thermal therapy using gold nanoparticles, J. Phys. Chem. C. 120 (2016) 4691–4716. https://doi.org/10.1021/acs.jpcc.5b11232.

[39] L. Guerrini, R.A. Alvarez-Puebla, N. Pazos-Perez, Surface modifications of nanoparticles for stability in biological fluids, Materials (Basel). 11 (2018) 1154. https://doi.org/10.3390/ma11071154.

[40] S. Salmaso, P. Caliceti, Stealth properties to improve therapeutic efficacy of drug nanocarriers, J. Drug Deliv. 2013 (2013) 374252. http://dx.doi.org/10.1155/2013/374252.

[41] VitroCom | Square - Miniature Hollow Glass Tubing (VitroTubes^{TM}), (n.d.). https://www.vitrocom.com/categories/view/70/Square-Miniature-Hollow-Glass-Tubing (accessed June 15, 2020).

[42] Teledyne QImaging Home - Teledyne Photometrics, (n.d.). https://www.photometrics.com/qimaging (accessed June 15, 2020).

[43] Maya2000 Pro Series Spectrometer | Ocean Insight, (n.d.). https://www.oceaninsight.com/products/spectrometers/high-sensitivity/maya-series/ (accessed June 15, 2020).

[44] Y. Prokazov, E. Turbin, A. Weber, R. Hartig, W. Zuschratter, Position sensitive detector for fluorescence lifetime imaging**,** J. Instrum.9 (2014) C12015-C12015. https://doi.org/10.1088/1748-0221/9/12/C12015

[45] T. Chakraborty, I. Chakraborty, S. Ghosh, Sodium carboxymethylcellulose - CTAB interaction: A detailed thermodynamic study of polymer - Surfactant interaction with opposite charges, Langmuir. 22 (2006) 9905–9913. https://doi.org/10.1021/la0621214.

[46] L. Schoutteten, P. Denjean, J. Faure, R.B. Pansu, Photophysics of calcium green 1 in vitro and in live cells, Phys. Chem. Chem. Phys. 1 (1999) 2463–2469. https://doi.org/10.1039/a900584f.

[47] Y. Bo, J. Fan, S. Yan, M. Ding, J. Liu, J. Peng, L. Ding, Surfactant modulation effect on the fluorescence emission of a dual-fluorophore: Realizing a single discriminative sensor for identifying different proteins in aqueous solutions, Sensors Actuators, B Chem. 295 (2019) 168–178. https://doi.org/10.1016/j.snb.2019.05.078.

[48] J. Fan, L. Qi, Y. Li, Q. Tang, L. Ding, Y. Fang, A single probe-based sensor array for fingerprinting biothiols in serum and urine via surfactant modulation strategy, Sensors Actuators, B Chem. 301 (2019) 127144. https://doi.org/10.1016/j.snb.2019.127144.

[49] P.P. Infelta, M. Grätzel, J.K. Thomas, Luminescence decay of hydrophobic molecules solubilized in aqueous micellar systems. A kinetic model, J. Phys. Chem. 78 (1974) 190–195. https://doi.org/10.1021/j100595a021.

[50] H. Laguitton-Pasquier, R. Pansu, J.P. Chauvet, P. Pernot, A. Collet, J. Faure, 10,10′-bis(2-ethylhexyl)-9,9′-bianthryl (BOA) molecule: The first free aromatic probe for the core of micelles, Langmuir. 13 (1997) 1907–1917. https://doi.org/10.1021/la960708k.